NUMERICAL INVESTIGATION OF DISTRIBUTED ROUGHNESS EFFECTS FOR TRANSIENT FLOW

Takuto Ogawa
Institute of Fluid Science
Tohoku University
2-1-1, Katahira, Aoba-ku, Sendai, 980-8577, Japan
takuto.ogawa@tohoku.ac.jp

Aiko Yakeno
Institute of Fluid Science
Tohoku University
2-1-1, Katahira, Aoba-ku, Sendai, 980-8577, Japan
aiko.yakeno@tohoku.ac.jp

ABSTRACT

Direct numerical simulations (DNSs) were performed for flow near the wall surface with a distributed micro roughness (DMR) arrangement with the roughness density. The Reynolds number was set to $Re_{\delta_s} = 3,535$ based on the boundary layer thickness at the inlet boundary (δ_s), with reference to the previous studies (Hamada *et al.* (2022, 2023)). The lengths of the computational domain in the streamwise and spanwise directions are $L_{x,\delta_s} = 56.5$ and $L_{y,\delta_s} = 11.3$, respectively. The artificial disturbance was added at the inlet boundary to induce Tollmien-Schlichting (T-S) wave. DMR is installed the wall surface at $2.8 \le x_{\delta_s} \le 42.4$, $0 \le y_{\delta_s} \le 11.3$. The drag coefficient ($C_f$) reduction effect of the roughness density were investigated by DNSs. The results of DNSs showed that the DMR with the appropriate roughness density achieves the C_f reduction in comparison with the flat plate case. The DMR of appropriate density gradually collapses the large-scale vortex structure generated by the T-S wave. The gradual collapse of the large-scale vortex structure suppresses the abrupt fluctuation in C_f and increase in TKE, thus achieving the C_f reduction.

INTRODUCTION

Innovative technologies to improve aircraft aerodynamics are needed to reduce environmental impact and achieve sustainable air transportation in the face of future aviation demand growth (ICAO (2016)). In general, skin friction drag is one of the most significant aerodynamic drag farm for commercial aircraft. Therefore, it is expected that methods to radically reduce skin friction drag will be developed. Riblets, one of the methods to achieve friction drag, can reduce friction drag by up to several percent under ideal flow conditions (Walsh *et al.* (1989)). However, friction drag increases when the deviation between the streamwise direction and the riblet direction exceeds a certain level. In addition, it is difficult to place a riblet on an aircraft because the fuselage and wings are three-dimensionally curved and the wing angle is set back. Tani proposes that hydrodynamically smooth roughness (Distributed Micro Roughness, DMR) has the effect of reducing friction drag (Tani (1988)). The smooth roughness is the roughnesses lower than low viscosity ($Re_k < 6$) . In recent years, with the development of numerical and measurement techniques, the characteristics of distributed micro roughness (DMR), including smooth roughness, has been analyzed. Several studies have been shown that changes in friction drag are greatly affected not only by the height of the DMR but also by its shape (Nugroho *et al.* (2021); Jelly & Busse (2019)). Hamada *et al.* (2022) have been analyzed the mechanism by which DMR reduces friction drag by performing DNS for the spanwise uniform sinusoidal roughness surface, the sandy roughness surface based on the actual sandpapers, and the randomly arranged roughness surface based on the Gaussian distribution. The result shows that the DMR based on sandpaper have a high drag reduction effect. At present, artificial creation of shapes that exceed the effect of the sandpaper case has not been achieved. And, the effects of the height, diameter and density of each roughness on the flow have not been investigated. In this study, DNSs of the flow over several DMRs are performed using the roughness density as a parameter. The artificial shapes based on the randomly arranged Gaussian distribution, which can simulate sandpaper, are used to quantitatively set the roughness density. The roughness densities are validated in a lower density range than in case of the previous studyHamada *et al.* (2022) in order to analyze of the influence of each roughness. The effect of the roughness density on the flow is evaluate in terms of the drag reduction.

PROBLEM SETTING

The analysis target is the flow near the wall surface with the smooth surface and the DMR. Figure 1 shows an overall flow field. The Reynolds number is set to $Re_{\delta_s} = 3,535$ based on the boundary layer thickness at the inlet boundary (δ_s). Note that the physical quantities with subscript δ_s are normalized by δ_s. The lengths in the streamwise, spanwise, and wall-normal direction are set to $L_{x,\delta_s} = 56.5$, $L_{y,\delta_s} = 11.3$, and $L_{z,\delta_s} = 28.3$, respectively. At the inlet boundary, a artificial disturbance is added to induce T-S wave. The shape of roughness is defined by a Gaussian function. Each roughness is randomly distributed in the range of $2.8 \leq x_{\delta_s} \leq 42.4$. The density of roughness is expressed as ρ_{δ_s}, the number of roughness per standard area. Therefore, the wall shape of DMR is expressed by the height h from the reference surface, as shown in Eq. 1. Figure 1 shows a example of the DMR. The density and height are set to $\rho_{\delta_s} = 1$ and $h_{\delta_s} = 1$, respectively. In this study, four DMRs are discussed as shown in Tbl. 1, and the effect of each DMR on the drag reduction is discussed. For example, $\rho_{\delta_s} = 1$ is the case where one roughness is distributed per 1 $[{\delta_s}^2]$. Thus, $\rho_{\delta_s} = 1/9$ is the case where one roughness is distributed per 9 $[{\delta_s}^2]$. The hight is set to $h_{\delta_s} = 0.141$ which is one of the effective values and confirmed in the previous study (Hamada *et al.* (2022, 2023)). The diameter of the each roughness is set to $\phi_{\delta_s} = 1/3$. These values are adjusted so that the effects of individual roughnesses could be assessed to some extent, even if the roughnesses are overlappingly distributed.

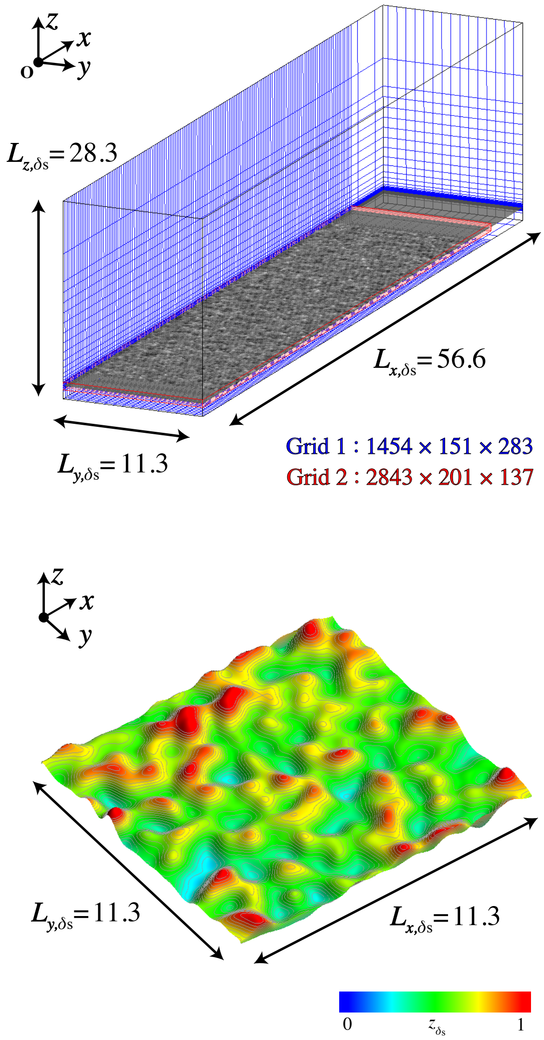

Figure 1: Computational grids and an example of gaussian roughness surface ($\rho_{\delta_s} = 1$, $\phi_{\delta_s} = 1$, $0 \leq h_{\delta_s} \leq 1$).

$$h(x,y) = \sum_{i=1}^{N} \alpha_i \exp\left(-\frac{(x-x_i)^2 + (y-y_i)^2}{2\sigma^2}\right) \tag{1}$$

Table 1: DMR conditions for computational cases.

ρ_{δ_s}	ϕ_{δ_s}	h_{δ_s}
1/9, 1, 9, 25	1/3	[-0.141:0.141]

NUNERICAL METHODS

The governing equations the fluid dynamics are the unsteady three-dimensional compressible Navier-Stokes equations. The 6th-order compact difference scheme is used for spatial differencing of the metric, jacobian, convective and viscous terms. The scheme is higher spatial accuracy and resolution than conventional compressibility schemes. The three-step total variation diminishing (TVD) Runge-Kutta method is used for time integration. The low-pass explicit filter is applied at the outlet boundary of the computational domain. Figure 1 shows computational grids used in this study. Grid nesting is applied to capture turbulence with high accuracy while reducing the computational cost. The number of grid points in Zone 1 for the entire computational domain and Zone 2 for the area near the DMR are approximately 60 and 80 million, respectively. The Volume Penalization (VP) method is used for represent the complex three-dimensional shape of the DMR (Liu & Vasilyev (2007)). Solid wall condition is applied to smooth surface boundaries located upstream and downstream of the DMR. At the inlet boundary, the streamwise and wall-normal velocities are calculated by the Blasius equation for a flat plate in uniform laminar flow are given, and the density and pressure are set to the same values as in the freestream. In addition, the vertical wall velocity is added as a artificial disturbance to induce T-S wave. At the outlet boundary, the density and pressure are free conditions (Dirichlet boundary conditions). At the far boundary in the wall-normal direction, the pressure and streamwise velocity are fixed to their free flow values, and the wall vertical velocity and spanwise velocity are free conditions. At the spanwise boundaries, the periodic conditions are applied. In-house code LANS3D is used for solving the unsteady three-dimensional compressible Navier-Stokes equations (Fujii (1990)). Each case is calculated until the downstream section transitions to turbulence and stabilises, and from there to $tU_\infty/\delta_s = 100$ in order to take a time average.

RESULTS AND DISCUSSION

Figures 2 and 3 show the integrated values of the drag coefficient (C_f) and the turbulent kinetic energy (TKE) along the vertical direction at each x_{δ_s} position for the flat plate and DMR cases, respectively. In each case, fluctuation of C_f due to T-S wave effects are observed near the inlet boundary. In the flat plate case, the fluctuation are observed up to $x_{\delta_s} \sim 30$, with a maximum peak at $x_{\delta_s} \sim 25$. Thereafter, C_f decreases moderately as it moves downstream. A similar tendency could be observed for TKE. The position of the maximum peak in TKE coincides with that of the maximum peak in C_f. This position also coincides with the position where the large-scale vortex structure collapses, as described below, and a relationship between the collapse of the vortex structure and the increase in C_f could be inferred. In the DMR cases, the tendency of C_f and TKE are slightly different from those in the flat plate case. In each case, C_f is higher than in the flat plate case at $10 \lesssim x_{\delta_s} \lesssim 20$. At $x \sim 15$, C_f in the DMR cases is about 10 times higher than that in the flat plate cases. However, the subsequent change is relatively gradual. The DMR cases do not have a high peak as in the flat plate case, and in many cases the value remains low. A similar tendency is observed in TKE. Figure 4 shows C_f integrated along with the streamwise direction ($I_{\Delta C_f}$) in each case. In the flat plate case, I_{C_f} get lower value than DMR cases until $x_{\delta_s} \sim 20$ where the large-scale vortex structure maintains its structure. However, I_{C_f} increases from $x_{\delta_s} \sim 30$ where the vortex structure collapses. Finally, the case of $\rho_{\delta_s} = 1$ has the lowest $I_{\Delta C_f}$. Therefore, it was shown that the DMR with the appropriate roughness density achieves C_f reduction.

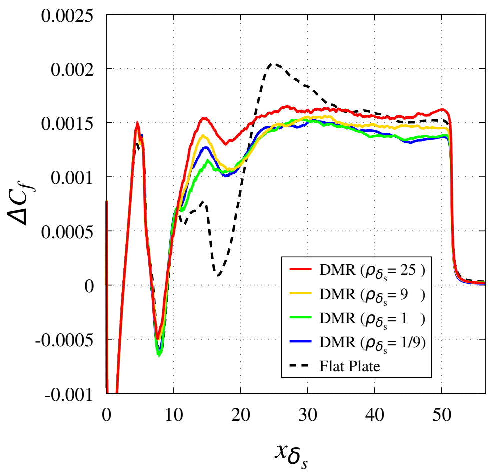

Figure 2: Decomposed (ΔC_f) value along the x direction.

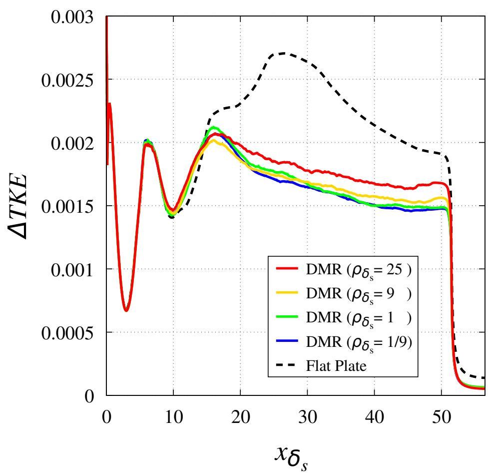

Figure 3: Decomposed integral value of the turbulent kinetic energy (ΔTKE) for the z direction at each position in the streamwise direction.

$$\Delta C_f = 2\int_0^{\infty} 2(1-z)(-\overline{u'w'})dz, \tag{2}$$

$$\Delta TKE = \int_0^{\infty} (\overline{u_i'' u_i''}/2)dz, \tag{3}$$

$$I_{\Delta C_f} = \int_{x_s}^{x_e} \Delta C_f dx, \quad (x_s = 0,\, x_e = L_{x_{\delta_s}}) \tag{4}$$

Since the DMRs cases have similar trends, the case of $\rho_{\delta_s} = 1$ is used as the representative case. Figure 5 shows the

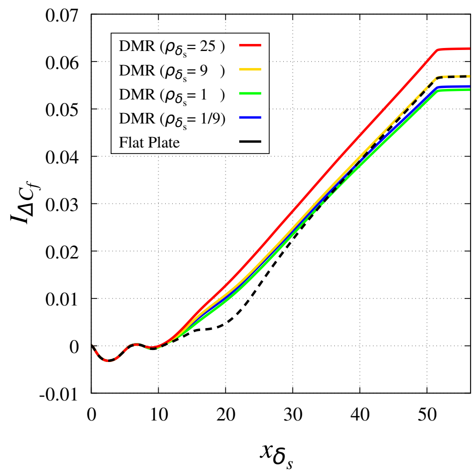

Figure 4: Integral value of the ΔC_f along the x direction.

instantaneous flow field over the wall surface for the flat plate and DMR ($\rho_{\delta_s} = 1$) cases. The isosurfaces are the second invariant of the velocity gradient tensor ($Q_{\delta_s} = 0.2 \times 10^{-4}$), colored by the streamwise velocity normalized by freestream velocity ($0 \leq u/U_\infty \leq 1$). In both cases, the advection of large-scale spanwise vortex structures due to T-S wave are observed the upstream. In the flat plate case, the large-scale vortex structures are maintained for a relatively long time. The large-scale vortex structures are locally merging, which causes C_f to fluctuate significantly. Subsequently, a deformation of the large-scale vortex structure is observed at $x \sim 25$. This position corresponds to the maximum peak for C_f. The result suggests that structural changes in the large-scale vortex structure contribute to an increase in C_f. In the DMR ($\rho_{\delta_s} = 1$) cases, the large-scale vortex structures gradually collapse from upstream. The fluctuation of C_f is smaller than in the flat plate case. Therefore, the speed of deformation and collapse of the large-scale vortex structure is considered to influence the variation of C_f. The flow then transitions to turbulence as it moves downstream. The maximum peak of C_f as in the flat plate case is not observed and the curve remains flat afterwards. In the flat plate case, the influence of the large-scale vortex structure remains downstream and vortices of relatively large scale are distributed. In the DMR cases, on the other hand, the vortex scale is relatively small. In both cases, C_f varies moderately, but there are differences in its value. The differences are presumably caused by differences in the scale of the distributed vortex structures.

CONCLUSIONS

DNSs of the flows over the several distributed micro roughnesses (DMRs) with roughness density as a parameter was performed to analyze the mechanism by which DMR achieves the drag reduction. DMRs with appropriate roughness density could suppress rapid fluctuations in C_f by gradually collapsing the large-scale vortex structure generated by the T-S wave. The scale of the vortex structures in the downstream turbulent region is also smaller than in the case of the flat plate, which is also considered to be a contributing factor for C_f reduction. In the future works, we will investigate the

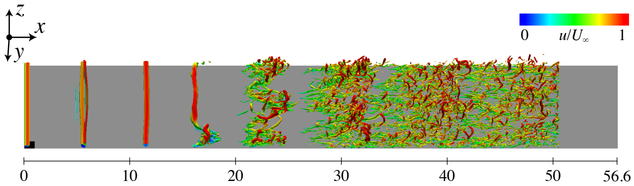

(a) Flat plate

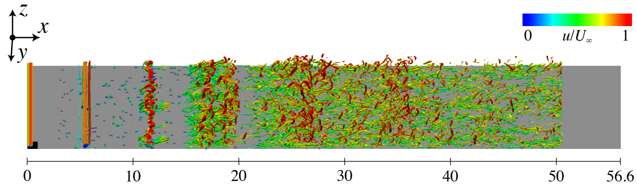

(b) DMR ($\rho_{\delta_s} = 1$)

Figure 5: Instantaneous flow field in cases of flat plate and DMR ($\rho_{\delta_s} = 1$).

effect of other parameters such as hight, and we will extract a feature value of DMR to estimate the influence of the DMR on the flow field.

ACKNOWLEDGEMENT

Numerical simulations were performed on the “AFINITY” supercomputer system at Institute of Fluid Science, Tohoku University. This work was supported by NEDO of Japan (JPNP20010). A. Y. appreciates the support of the KAKENHI (19K14880, 19KK0373, and 23H01335) from JSPS by MEXT of Japan and JST FOREST Program (JPMJFR222R).

REFERENCES

Fujii, K. 1990 Developing an accurate and efficient method for compressible flow simulations -example of cfd in aeronautics-. *The Proceedings: Fifth International Conference on Numerical Ship Hydrodynamics* .

Hamada, S., Yakeno, A. & Obayashi, S. 2022 Ultra-fine roughness effect on transition delay using direct numerical simulation. In *Proceedings of 12th International Symposium on Turbulence and Shear Flow Phenomena (TSFP 2022)*.

Hamada, S., Yakeno, A. & Obayashi, S. 2023 Drag reduction effect of distributed roughness on the transitional flow state using direct numerical simulation (unpublished observation). *International Journal of Heat and Fluid Flow* .

ICAO, International Civil Aviation Organization 2016 A proposal from icao (url: https://aviationbenefits.org/blog/2016/04/a-proposal-from-icao/, 30 sep, 2023). *Tech. Rep.*.

Jelly, T. O. & Busse, A. 2019 Reynolds number dependence of reynolds and dispersive stresses in turbulent channel flow past irregular near-gaussian roughness. *International Journal of Heat and Fluid Flow* **80**.

Liu, Q. & Vasilyev, O. V. 2007 A brinkman penalization method for compressible flows in complex geometries. *Journal of Computational Physics* **227** (10), 946–966.

Nugroho, B., Monty, J. P., Utama, I. K. A. P., Ganapathisubramani, B. & Hutchins, N. 2021 Non-k-type behaviour of roughness when in-plane wavelength approaches the boundary layer thickness. *Journal of Fluid Mechanics* **911**.

Tani, I. 1988 Drag reduction by riblet viewed as roughness problem. *Proceedings of the Japan Academy* **64**, 21–24.

Walsh, M. J., Sellers III, W. L. & McGinley, C. B. 1989 Riblet drag at flight conditions. *Journal of Aircraft* **26** (6).